Photodissociation of 2-Iodoethanol within the A Band

V. Alvin Shubert, Maria Rednic,[†] and Stephen T. Pratt*

Argonne National Laboratory, Argonne, Illinois 60439

Received: April 9, 2009; Revised Manuscript Received: June 26, 2009

The photodissociation of 2-iodoethanol was studied within the A ($\sigma^* \leftarrow$ n) absorption band at several wavelengths between 253 and 298 nm, and the velocity distributions and angular distributions of the photofragments were characterized by using velocity-map ion imaging. The two dominant dissociation channels correspond to the production of the 2-hydroxyethyl radical, C_2H_4OH, and $I(^2P_{3/2})$ and $I^*(^2P_{1/2})$, and in both channels, approximately 50% of the available excess energy is partitioned into translational energy of the fragments. The branching fractions for the I and I* channels at 266 nm were determined by using a combination of (1) the translational energy distributions for the separate I and I* channels determined by two-photon resonant, three-photon ionization, (2) the distributions for the combined I + I* channels determined by single-photon ionization at 118 nm, and (3) the relative photoionization cross sections of I and I* at 118 nm. Evidence was observed for either the secondary decomposition of C_2H_4OH, the photodissociation of C_2H_4OH, or the dissociative ionization of the C_2H_4OH radicals produced in the I channel. These mechanisms are also discussed.

I. Introduction

Reactions between alkenes and OH radicals play important roles in combustion flames[1−11] and are the primary pathway for alkene degradation in the atmosphere.[3−7,12,13] The hydroxyalkyl radicals represent an important class of intermediates in these reactions, and an understanding of the energetics and decay processes for these radicals can provide insight into the reaction mechanisms. The reaction of OH with ethylene, the simplest alkene, is of particular interest, and has been the subject of several recent theoretical studies.[7−11] The 2-hydroxyethyl radical plays an important role in this reaction, and has been the subject of a number of recent studies as well.[2,3,12−15] The photodissociation of 2-haloethanols provides a direct means to produce this radical,[14,15] and by varying the photodissociation wavelength and the halogen atom, it is possible to produce the radicals with a wide range of internal energies. In some instances, the radicals formed by photodissociation have sufficient internal energy to undergo secondary dissociation to C_2H_4 + OH, and this process was studied as well.

Hintsa, Zhao, and Lee studied the photodissociation of 2-bromo- and 2-chloroethanol at 193 nm by using translational spectroscopy of the photofragments.[15] Using the known photon energy and the C−X bond dissociation energies, the translational energy distributions obtained from the Cl and Br fragments provided a measure of the internal energy of the C_2H_4OH cofragment. The halogen atom distributions indicated that a significant fraction of the C_2H_4OH was formed with sufficient energy to undergo secondary dissociation. For 2-chloroethanol, neither C_2H_4OH nor its fragments were observed with sufficient intensity to study directly. For 2-bromoethanol, Hintsa et al.[15] found both stable C_2H_4OH fragments as well as species produced by secondary fragmentation to C_2H_4 + OH. Interestingly, they observed significant signal from C_2H_4OH having an internal energy well in excess of its fragmentation threshold. They ascribed this C_2H_4OH signal to highly rotationally excited radicals formed as a result of the dynamics of the parent photodissociation process. In this case, the rotational energy of the C_2H_4OH is ineffective at overcoming the barrier for dissociation to C_2H_4 + OH, and the radical does not fragment.

Chandler et al.[14] also studied the photodissociation of 2-bromoethanol at 202 nm by using ion imaging techniques. In these experiments, resonance-enhanced multiphoton ionization was used to detect ground state Br $^2P_{3/2}$ and spin−orbit excited Br $^2P_{1/2}$ separately, and the ion images provide both the translational energy distributions and the angular distributions of the fragments. Chandler et al.[14] also concluded that the C_2H_4OH was formed in high rotational levels. Subsequently, Sapers and Hess[3] studied the photodissociation of 2-bromoethanol and 2-iodoethanol at 202 and 266 nm, respectively, by using laser-induced fluorescence to monitor the OH fragment produced by the secondary decomposition of C_2H_4OH. Their results were consistent with the C_2H_4OH being produced in highly excited rotational levels. Although the C−I bond energy is smaller than the C−Br bond energy, the internal energy distribution of the C_2H_4OH in the iodoethanol experiments was peaked at much lower energy than in the bromoethanol experiments as a result of the significantly lower photon energy. Sapers and Hess[3] estimated that the fraction of secondary dissociation of C_2H_4OH in the iodoethanol experiments was only 0.02 of that in the bromoethanol experiments, corresponding to about 1% of the total. Sapers and Hess[3] also found convincing evidence that the C_2H_4OH produced by the photodissociation of iodoethanol efficiently absorbed 266 nm light, resulting in photodissociation of the C_2H_4OH to C_2H_4 + OH through the absorption of an additional photon. Interestingly, earlier work of Anastasi et al.[16] suggested that absorption by C_2H_4OH is quite weak at 266 nm, and only increases substantially at shorter wavelengths. However, it is possible that the internal energy of the C_2H_4OH in the Sapers and Hess experiments leads to enhanced absorption at 266 nm.

In the present study, we have investigated the photodissociation of 2-iodoethanol at 266 nm, and at several additional wavelengths between 258 and 298 nm, to provide additional insight into the dissociation process. In particular, we have used a combination of resonance-enhanced multiphoton ionization

[†] Current address: University of Illinois Urbana−Champaign, Urbana, Illinois 61801.

10.1021/jp903301g CCC: $40.75
Published on Web 07/17/2009

and velocity-map ion imaging to record the translational energy distributions and photofragment angular distributions in the I $^2P_{3/2}$ and I* $^2P_{1/2}$ channels separately. We have also used a combination of these techniques and single-photon ionization to determine the branching fractions for the two channels at 266 nm. Finally, we have used a comparison of the I and I* translational energy distributions with that recorded by single-photon ionization of the C_2H_4OH radical to estimate the extent of secondary dissociation of the latter.

II. Experiment

Velocity-map ion imaging was employed as the primary detection scheme for the data presented in this work. The apparatus used for this report has been previously detailed[17,18] and is described only briefly here. Velocity-map ion images were obtained with a modified time-of-flight mass spectrometer fitted with an electrostatic immersion lens similar to that described by Eppink and Parker.[19] The molecular sample was introduced into the chamber with a pulsed valve (General Valve Series 9, 10 Hz) used to produce a supersonic molecular jet, which was collimated by a 2 mm skimmer to produce the molecular beam. For the present experiments, the 2-iodoethanol sample holder, pulsed valve, and gas line connecting them were heated to approximately 60−70 °C. This heating increased the 2-iodoethanol vapor pressure to ∼7.5 Torr (estimated using $\Delta_{vap}H_m°(ICH_2CH_2OH) = 57.03$ kJ/mol,[12] and a boiling point of ∼170−175 °C). Helium was used as the carrier gas at a stagnation pressure of 1000−1500 Torr, resulting in a sample concentration of ∼0.5% of 2-iodoethanol in the molecular beam. For the trifluoro-iodomethane calibration images, the sample was held at room temperature and the concentration in the beam was ∼3%.

Either the frequency doubled output of a Nd:YAG pumped dye laser or the fourth harmonic (266 nm) output of a Nd:YAG laser initiated the photodissociation process, with the laser output crossing the molecular beam at a 90° angle in the interaction region of the spectrometer. A Glan-laser polarizer purified the light polarization, which was aligned perpendicular to the propagation direction of the molecular beam and parallel to the face of the ion detector. The dissociation fragments were photoionized either by a two-photon resonant, three-photon ionization with the same laser used for the photodissociation process or by single-photon ionization with vacuum ultraviolet (vuv) light at 118.2 nm. In the former method, photodissociation and two-photon resonant, three-photon ionization of the I or I* fragments were performed with a single laser tuned to one of the many atomic I two-photon resonances between 250 and 310 nm. In the latter method, the 266 nm light was used to photodissociate the sample and the 118.2 nm light was used for the detection of both atomic iodine and radical photofragments. The 118.2 nm vuv light was generated via nonresonant third-harmonic generation in Xe using the 354.7 nm third harmonic of a Nd:YAG laser. The photodissociation and vuv beams were counterpropagating and had the same linear polarization; the photodissociation pulse preceded the vuv pulse by 50 ns.

The photoions traveled the length of the flight tube and impinged on a dual-channel plate detector coupled to a phosphor screen. Detection of only the ions with the mass of interest was accomplished by gating the detector voltages. Ion images were obtained by viewing the phosphor screen with a standard video camera, and data acquisition was accomplished with a commercial ion-imaging system (McLaren Research, MR-2) that collected the raw image and generated a centroided image for each laser shot. Final images were recorded by averaging 10 000 to 40 000 laser shots. A series of digital delay generators synchronized to the detector camera controlled the timing of the molecular beam pulse, lasers, detector gating, and detection system.

The centroided two-dimensional images obtained in the experiments were symmetrized and reconstructed using either the BASEX[20] or pBASEX[21] programs. The translational energy distributions obtained from the reconstructions were calibrated with previously reported photofragment energies for the photodissociation of CF_3I.[18] The radial distributions were fit with Gaussian functions to determine the center of the vibrational distribution envelope produced by photodissociation. Assignment of these center positions to the average translational energies, $\langle E_{trans} \rangle$, was made by using those previously reported for CF_3I at several dissociation wavelengths. In general, calibration images for both the I and I* distributions from CF_3I were obtained on the same day as the iodoethanol image of interest, and the average conversion factor found from the I and I* images was used for the calibration of the 2-iodoethanol images. If only an I or I* image was available, then that conversion was used directly. If the calibration image was obtained at a previously unreported wavelength, then the peak of the CF_3I translational energy distribution was assigned to an appropriate vibrational quantum number, assuming excitation of a 700 cm^{-1} vibrational mode of CF_3. The accuracy of the final calibrated translational energy distributions is estimated to be approximately 350 cm^{-1} (43 meV), corresponding to approximately one pixel in the energy regime relevant for iodoethanol.

III. Background on the Absorption Spectrum

The photodissociation wavelengths used in the present study of iodoethanol fall in the middle of the A ← X band resulting from the σ^* ← n transition from a lone pair orbital of the I atom to the σ^* orbital centered on the C−I bond.[22,23] The analogous transition has been the subject of numerous studies on the alkyl halide molecules,[24−38] and only a brief review of relevant details is provided here. The first weak absorption band of ethanol is observed at much shorter wavelengths,[39] beginning to rise above the background at ∼200 nm, and thus, for iodoethanol at 266 nm, the σ^* ← n transition should be well-isolated from all other features. However, for 2-bromoethanol and 2-chloroethanol, the σ^* ← n transition is shifted to shorter wavelengths, and near 200 nm and below, the character of the absorption band is expected to be somewhat more complicated.

The electron configuration resulting from the σ^* ← n excitation results in five spin−orbit states: two ($^3Q_{0-}$ and $^3Q_2$) that are forbidden via single-photon transitions,[40] and three ($^1Q_1$, $^3Q_{0+}$, and $^3Q_1$) that are allowed. The $^1Q_1$ and $^3Q_1$ states correlate diabatically with production of a ground state radical and ground state I $^2P_{3/2}$ atom.[22,23] The $^3Q_{0+}$ state correlates diabatically with production of a ground state radical and a spin−orbit excited I* $^2P_{1/2}$ atom[22,23] (referred to as I*). Studies of a large number of alkyl halides indicate that the $^3Q_{0+}$ ← X transition dominates the A band, although weaker absorption due to the $^1Q_1$ ← X transition and $^3Q_1$ ← X transitions occurs in the blue and red wings of the band, respectively. The transition dipole moment for the $^3Q_{0+}$ ← X transition is approximately parallel to the C−I bond, while those for the $^1Q_1$ ← X and $^3Q_1$ ← X transitions are approximately perpendicular to the C−I bond. Thus, the A ← X band has predominately parallel character.

A conical intersection occurs between the $^3Q_{0+}$ and $^1Q_1$ surfaces along the C−I stretch. In the C_s symmetry of 2-iodo-

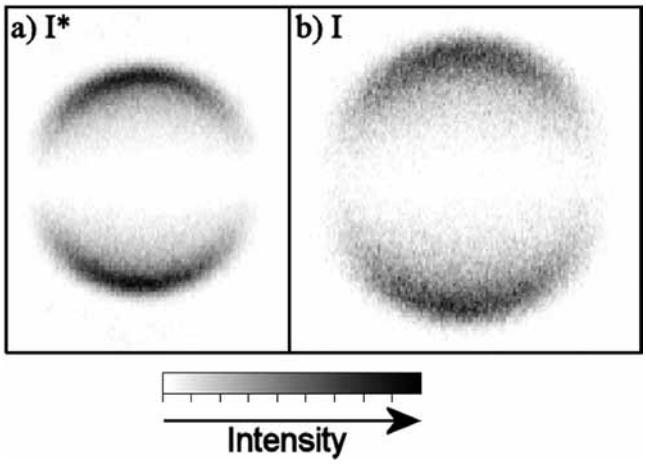

Figure 1. Images of I atoms from dissociation of 2-iodoethanol at (a) 266.622 nm and (b) 266.490 nm corresponding to resonant two photon + one ionization transitions from the I*($^2P_{1/2}$) and I($^2P_{3/2}$) states, respectively.

ethanol, this results in an avoided crossing, such that the $^3Q_{0+}$ surface is ultimately adiabatically correlated with $C_2H_4OH + I$ $^2P_{3/2}$ and the $^1Q_1$ surface is correlated with $C_2H_4OH + I^*$ $^2P_{1/2}$. The extent of diabatic crossing through this intersection provides insight into the relative shapes of the two surfaces and the interaction between them. Because the excitation of the $^3Q_{0+}$ and $^1Q_1$ surfaces has parallel and perpendicular behavior, respectively, and because prompt dissociation is expected for 2-iodoethanol excited within the A band, the photofragment angular distributions can provide insight into the adiabaticity of the surface crossing.

IV. Results and Discussion

A. I and I* Distributions. Figure 1 shows typical I atom fragment images collected following photodissociation of 2-iodoethanol near 266 nm. The images were obtained by selectively detecting I atoms in either the spin−orbit excited state, I*($^2P_{1/2}$), or ground state I($^2P_{3/2}$), by using two-photon resonant, three-photon ionization via the ($^3P_1$)7p[1]$_{1/2}$ and ($^3P_2$)7p[2]$_{3/2}$ intermediate states,[41] respectively. The highest intensities in both images occur along the polarization axis of the laser, which is consistent with the dominant $^3Q_{0+} \leftarrow X$ parallel transition.

Figures 2 and 3 present the translational energy distributions resulting from reconstruction of the I $^2P_{3/2}$ and I* $^2P_{1/2}$ images, respectively, obtained at several photodissociation wavelengths. The relevant data extracted from the distributions is summarized in Table 1. The average translational energies, $\langle E_{trans} \rangle$, of each distribution were determined by fitting a Gaussian function to the distributions. As expected, the average translational energy, $\langle E_{trans} \rangle$, increases with increasing dissociation photon energy in both the I and I* channels. The fraction of excess energy partitioned into E_{trans} is approximately independent of the photodissociation wavelength. This result is quantified by the ratio of $\langle E_{trans} \rangle$ to the total available energy, E_{avl}, which was determined from the conservation of energy equation:

$$E_{avl} = h\nu - D_0(I-CH_2CH_2OH) - E_{so} \quad (1)$$

In this equation, $h\nu$ is the energy of the dissociation photon, $D_0(I-CH_2CH_2OH)$ the dissociation energy of the C−I bond in 2-iodoethanol [D_0(I-CH_2CH_2OH) = 19120 cm^{-1}],[12] and E_{so} is the spin orbit energy of the I atom[41] (E_{so} = 0 cm^{-1} for I $^2P_{3/2}$ and E_{so} = 7603.15 cm^{-1} for I* $^2P_{1/2}$).

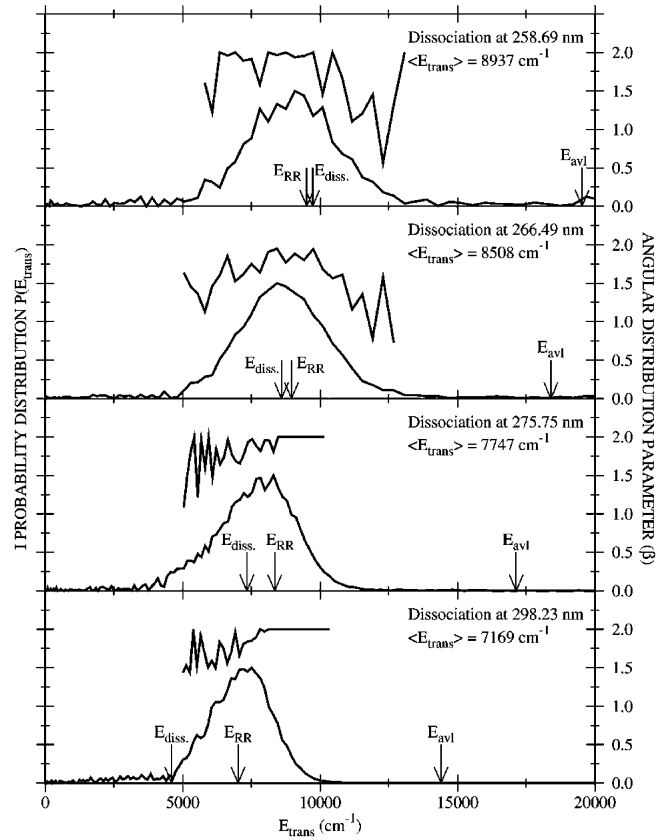

Figure 2. Total translational energy distributions obtained from detection of I($^2P_{3/2}$) state I atoms over a range of dissociation wavelengths along with corresponding photofragment anisotropy parameter, β, plotted from 0 to 2 (rather than −1 to 2) above each $P(E_{trans})$. E_{avl}, E_{RR}, and E_{diss} refer, respectively, to the available energy (see eq 1), the predicted energy from the rigid radical model, and the maximum total translational energy for which the radical retains enough internal energy to undergo secondary dissociation to C_2H_4 + OH.

Table 1 shows that the fraction of energy partitioned into translational energy remains constant over the wavelength region investigated, resulting in $\langle E_{trans} \rangle / E_{avl} = 0.52 \pm 0.01$ for the I* product channel and $\langle E_{trans} \rangle / E_{avl} = 0.47 \pm 0.02$ for the I channel. Thus, the fraction of energy partitioned into internal energy of the radical, $\langle E_{int} \rangle / E_{avl}$, is also about 0.5 in both channels.

That approximately half of the available energy is partitioned into internal degrees of freedom of the 2-hydroxyethyl radical stands in contrast to the energy partitioning in methyl radical from methyl iodide photodissociation, where only about 10% of the available energy is partitioned to the internal degrees of freedom.[38,42,43] However, the partitioning in iodoethanol is comparable to that in the photodissociation of less symmetric, longer chain alkyl iodides such as ethyl iodide[36,44,45] ($\langle E_{int} \rangle / E_{avl}$ = ∼0.74 for I* and ∼0.63 for I as averaged from several studies), *n*-propyl iodide[36,43,46] ($\langle E_{int} \rangle / E_{avl}$ = ∼0.54 for I* and ∼0.47 for I), and *i*-propyl iodide[36,43,46] ($\langle E_{int} \rangle / E_{avl}$ = ∼0.4 to 0.6 for I* and ∼0.4 to 0.5 for I). The partitioning observed in the present study is also comparable to that previously measured for the photodissociation of 2-bromoethanol at 193 nm, where $\langle E_{int} \rangle / E_{avl} = 0.58$.[15]

The anisotropy parameters, β, as a function of total translational energy are plotted over the corresponding translational energy distributions in Figures 2 and 3. The β plots show that β is very near or at the limiting value of 2.0 over most of the nonzero part of the distributions. This behavior is consistent with excitation via a parallel transition (i.e., $^3Q_{0+} \leftarrow X$), followed

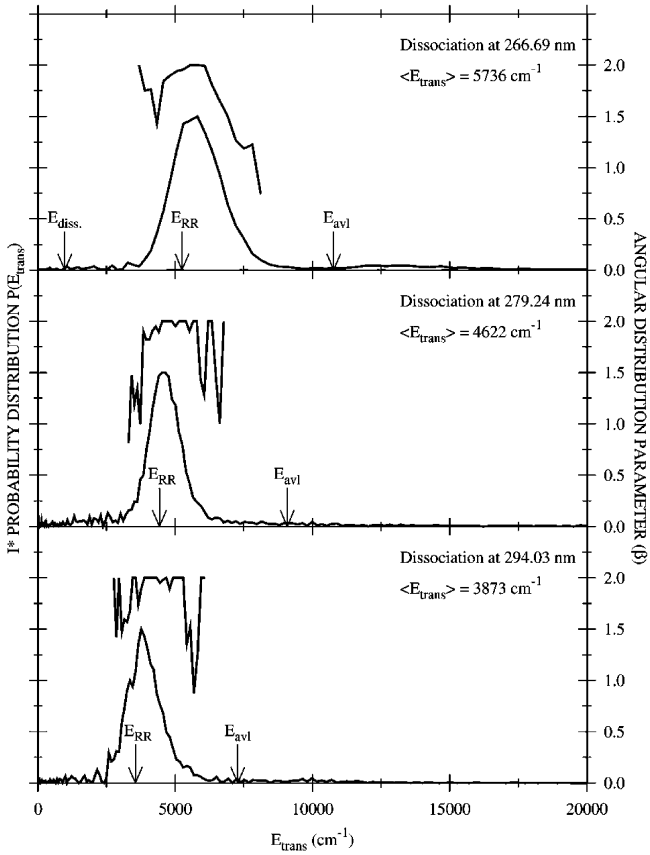

Figure 3. Translational energy distributions obtained from detection of I*($^2P_{1/2}$) state I atoms over a range of dissociation wavelengths along with corresponding photofragment anisotropy parameter, β, plotted from 0 to 2 (rather than −1 to 2) above each $P(E_{trans})$. E_{avl}, E_{RR}, and E_{diss} refer, respectively, to the available energy (see eq 1), the predicted energy from the rigid radical model, and the maximum total translational energy for which the radical retains enough internal energy to undergo secondary dissociation to C_2H_4 + OH.

by prompt dissociation. Small deviations from the limiting value toward smaller β are observed on the leading and trailing sides of the translational energy distributions. These deviations could result from a number of factors, including contributions from perpendicular transitions; however, the data are noisy in the regions of these deviations, and thus they may simply reflect the low signal level. In any event, the β plots suggest that the $^3Q_{0+} \leftarrow X$ transition carries the bulk of the oscillator strength in the wavelength region of interest here, a finding that is consistent with existing data on the alkyl iodides. In what follows, the interpretation of the data is presented only in terms of contributions from the parallel transition.

Although the $^3Q_{0+} \leftarrow X$ transition clearly dominates the absorption spectrum of 2-iodoethanol, there is substantial signal in both the I and I* dissociation channels. The $^3Q_{0+}$ state is diabatically correlated with the I* fragment and undergoes an avoided crossing with the $^1Q_1$ state; thus, it is adiabatically correlated with I ground state fragments. The production of I* fragments corresponds to diabatic dissociation on the $^3Q_{0+}$ surface, and the production of I corresponds to adiabatic evolution from the $^3Q_{0+}$ surface to the $^1Q_1$ surface. Thus, the branching fractions for I and I* can provide insight into the degree of adiabaticity or diabaticity in the dissociation process. To determine these branching fractions at 266 nm, we have recorded the image of the I and I* fragments together by using 118 nm light. We have then used the translational energy distribution resulting from this image, along with the separate I and I* distributions from the state-selected images, to determine the branching fractions as follows.

First, the distribution of I and I* determined at 118 nm was reconstructed by using the separate I and I* distributions obtained at 266.490 and 266.662, respectively, to determine the relative weights of the I and I* channels. The three dissociation wavelengths used for this comparison differ by less than 100 cm^{-1}, and it is assumed that the translational energy distributions are not affected substantially by this difference. [Note as well that the resolution in the images is at least three times this difference.] The comparison of the I and I* distribution obtained by using 118 nm light and the distribution reconstructed from the separate I and I* distributions is shown in Figure 4. The true branching fractions were then determined by integrating the separate areas of the I and I* peaks, and scaling them by the known value of 19.2 for the ratio of the photoionization cross sections of I and I* at 118.2 nm, which was determined previously.[17] The corrected I and I* signals were then used to calculate the branching fractions by dividing the signal in each channel by the total signal. This process yields

$$\Phi^* = \frac{I^*}{I + I^*} = 0.75 \pm 0.06 \qquad (2)$$

and

$$\Phi = \frac{I}{I + I^*} = 0.25 \pm 0.06 \qquad (3)$$

These values are similar to the branching fractions at 266 nm for several other alkyl iodides including methyl iodide ($\Phi^* = 0.76 \pm 0.02$), ethyl iodide ($\Phi^* = 0.72 \pm 0.02$), and *n*-propyl iodide ($\Phi^* \sim 0.7$). The similar value of Φ^* for iodoethanol indicates that the dissociation process exhibits a similar degree of adiabaticity (or similar degree of surface hopping) to the smaller alkyl iodides.

B. CH_2CH_2OH Radical Image at 266 nm. The large fraction of available energy partitioned into internal energy ($\langle E_{int} \rangle = \sim 7000-10500$ cm^{-1} over the range of photodissociation wavelengths used) naturally leads to the consideration of secondary dissociation pathways. The barriers to direct OH loss ($\sim$9800 cm^{-1})[7−11] or aliphatic H loss ($\sim$11 500 cm^{-1})[7−11] are sufficiently low that, as shown in Figure 2, some of the radicals with low translational energy formed by photodissociation at wavelengths shorter than 276 nm should have enough internal energy to undergo one of these secondary dissociation reactions.

In addition to these direct dissociation processes, some radicals are formed with enough internal energy to undergo isomerization reactions to CH_3CH_2O ($\sim$11 200 cm^{-1})[7−11] or to CH_3CHOH ($\sim$11 700 cm^{-1}).[7−10] In principle, these isomers may then undergo decomposition of their own (aliphatic H loss or C−C bond fission to CH_3 + CH_2O for CH_3CH_2O, aliphatic or hydroxy H loss for CH_3CHOH) as the energetic barriers to subsequent decomposition of these two isomers are below the isomerization barriers that led to their formation. Another reaction pathway leads to formation of H_2O and C_2H_3, although the most energetically favorable route requires H abstraction by the OH radical following decomposition to ethylene + OH. If this latter reaction occurs, it likely does so via a mechanism similar to the roaming atom or roaming radical mechanisms,[47] in which a very loosely bound OH radical abstracts an H atom from the CH_2CH_2 or CH_3CH moiety. Thus, the potential energy surface on which the ethene + OH radical reaction takes place

TABLE 1: Translational Energy Distribution Parameters

image	λ (nm)	E_{avl} (cm^{-1})	$\langle E_{trans}\rangle^a$ (cm^{-1})	$\langle E_{int}\rangle^a$ (cm^{-1})	$\langle E_{trans}\rangle/E_{avl}$	β	$E_{RR}{}^b$ (cm^{-1})	$E_{diss}{}^c$ (cm^{-1})
I*	294.033	7276	3873	3403	0.53	1.88±0.18	3544	−2524
	279.244	9077	4622	4455	0.51	1.95±0.06	4421	−723
	266.622	10 772	5736	5037	0.53	1.78±0.23	5247	972
I	298.230	14 400	7169	7232	0.50	1.84±0.17	7014	4600
	275.751	17 134	7747	9387	0.45	1.82±0.23	8346	7334
	266.490	18 394	8508	9887	0.46	1.72±0.15	8959	8594
	258.687	19 526	8937	10 589	0.46	1.88±0.17	9511	9726

[a] Multiple measurements yield an uncertainty of ±120 cm^{-1} for $\langle E_{trans}\rangle$ and $\langle E_{int}\rangle$. [b] E_{RR} corresponds to the total translational energy predicted by the rigid radical model. [c] E_{diss} corresponds to the maximum total translational energy that allows the radicals sufficient internal energy to dissociate.

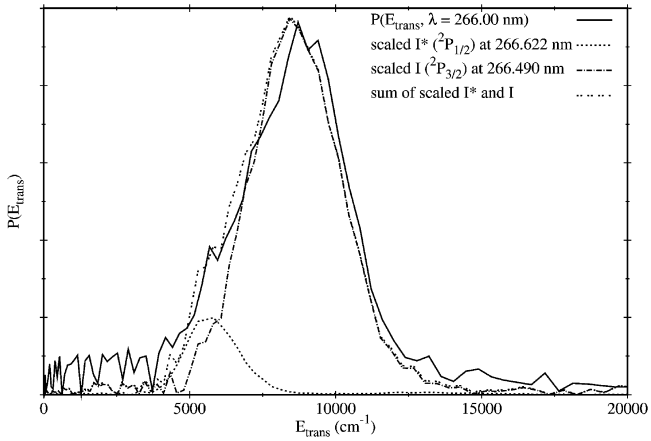

Figure 4. Translational energy distribution of I* + I atoms from photodissociation of 2-iodoethanol at 266 nm with 118 nm photoionization. Scaled I* and I atom distributions from resonant detection of each near 266 nm are used to reconstruct the I* + I distribution.

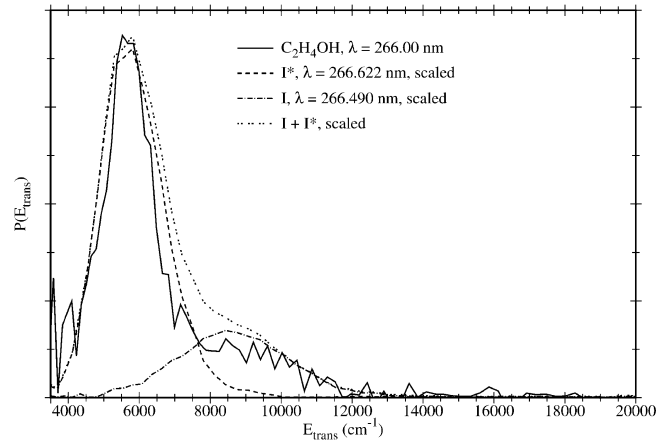

Figure 5. CH_2CH_2OH radical distribution and to scaled I* and I atom distributions from resonant detection of each near 266 nm. An I* branching fraction of 0.75 was used to predict the initial CH_2CH_2OH radical distribution prior to any secondary decomposition reactions.

can lead to a rich variety of dynamics and reaction products. Despite these possibilities, however, calculations by Klippenstein[7,48] of the branching fractions for the different dissociation pathways indicate that for the internal energies of interest here the C_2H_4 + OH channel is by far the dominant one, and that the others contribute less than 1% to the branching fractions.

In the present experiments, the energy of the ionization laser, 10.49 eV, is well above the ionization potential (IP) for the CH_2CH_2OH (IP ≤ 8.35 eV), CH_3CHOH (IP < 6.85 eV), and CH_3CH_2O (IP = 10.29 eV) isomers of C_2H_5O.[49] Thus, the isomers will not be distinguished in the mass spectra, but they could result in different translational energy distributions and angular distributions. Of the possible decomposition products, only methyl radical (IP = 9.84 eV) could in principle be detected, as the IPs of H (IP = 13.598 eV), OH (IP = 13.017 eV), H_2CO (IP = 10.89 eV), and C_2H_4 (IP = 10.514 eV) are higher than the photon energy.[50] However, no methyl radical was observed in our experiments.

Figure 5 shows the translational energy distribution from the reconstruction of the velocity-map image obtained by monitoring the $CH_2CH_2OH^+$ mass, along with the scaled I* and I distributions taken near 266 nm. The 118.2 nm laser light used for photoionization of the alkyl fragments can also initiate dissociative ionization of the 2-iodoethanol parent molecule, a process that produces a large signal that peaks at $E_{trans} = 0$ cm^{-1} and extends out to approximately 10 000 cm^{-1}. Thus, to obtain the distribution presented in Figure 5, images were collected with both the 266 nm photodissociation laser present and absent. The reconstructed velocity distribution obtained from the image with only the photoionization laser present was subtracted from that with both the photodissociation and photoionization lasers present to give the distribution in Figure 5. The bulk of the radical signal is correlated with the production of I* atoms, consistent with the previously determined I* branching fraction of $\Phi^* = 0.75$. This consistency also suggests that the detection efficiency of the CH_2CH_2OH radicals at 118.2 nm is not strongly dependent upon the internal energy of the radicals.

Assuming a barrier to C_2H_4 + OH bond dissociation energy of 9800 cm^{-1} (an average of the values reported by several studies[7−11]), the maximum total translational energy that allows the radicals sufficient internal energy to overcome this barrier and dissociate can be calculated at each photodissociation wavelength, and this maximum translational energy is denoted E_{diss}. For radicals formed in the I channel by photodissociation at 266 nm, E_{diss} = ∼8700 cm^{-1}. The corresponding values of E_{diss} at the other photodissociation wavelengths are provided in Table 1. From the ground state I distributions obtained with 266.490 nm photodissociation, approximately 53% of the I correlated radicals have translational energies less than 8700 cm^{-1}. To estimate the fraction of radicals undergoing secondary dissociation, the I* and I distributions obtained near 266 nm were scaled using $\Phi^* = 0.75$. Because the internal energies at 266 nm ($\langle E_{int}\rangle$ = 4920 cm^{-1}) of the I* correlated radical fragments should be insufficient for any secondary reactions to take place, the peak height of the sum of the scaled I* and I distributions was matched to the peak height of the radical distribution. These scaled distributions as well as their sum are also plotted in Figure 5. The scaled I* and I distributions reproduce the features of the radical distribution quite well; however, the I peak is enhanced relative to the corresponding feature in the radical distribution, indicating the presence of a secondary dissociation process in this channel.

If it is assumed that the radicals in the I* channel are stable, then subtracting the scaled I* distribution from the distribution

obtained from the radical image yields the distribution of radicals correlated with production of I atoms that remained stable following photodissociation. The difference between this distribution and the scaled I distribution indicates that approximately 45−60% of the radicals correlated with I atoms dissociate. This fraction corresponds to 11−15% of all of the radicals (i.e., radicals correlated with either I or I*) produced from 266 nm photodissociation. While the observed fraction of secondary dissociation of I correlated radicals is close to the expected value (~53%), the radical and I distributions in Figure 5 begin to diverge at $E_{trans} = \sim 9500$ cm^{-1}, corresponding to $E_{int} = \sim 8900$ cm^{-1}, significantly below the energy threshold for secondary dissociation of the radical. In addition, as discussed above, a significant fraction of this internal energy is expected to be tied up in rotations that are ineffective at overcoming the barrier to dissociation. Furthermore, there is no observed discontinuity (i.e., increase) in the fraction of dissociation at the secondary dissociation threshold. Thus, because the lowest dissociation barrier corresponds to $E_{trans} = 8700$ cm^{-1}, it is evident that most of the radical dissociation observed in the present experiments must be produced by absorption of one or more additional photons by the radical. This finding is consistent with the observations of Sapers and Hess,[3] who observed less than 1% secondary dissociation of the CH_2CH_2OH radicals; they concluded that some of the radicals were photofragmented by the absorption of an additional photon at 266 nm. Additional evidence against secondary decomposition of the C_2H_4OH comes from studies as a function of the delay between the pump (266 nm) and probe (118.2 nm) pulses. In particular, because the internal energy of the radicals is close to the dissociation threshold, the decomposition rate is expected to be slow. Experiments with pump−probe delays of 0−200 ns show no appreciable difference in the C_2H_4OH signal, further suggesting that secondary decomposition is not important on the time scale of this study.

Here, we consider two alternative explanations for the present observations; neither of these is expected to show a dependence on the pump−probe delay. First, as discussed by Sapers and Hess, the radical could absorb one or more additional 266 nm photons, and second, the radical could obtain additional internal energy upon photoionization at 118 nm, and thus undergo dissociative photoionization. These two possibilities are now discussed in more detail.

Sapers and Hess reported that ~99% of CH_2CH_2OH radicals remained stable following 266 nm photodissociation[3] but also provided convincing evidence that CH_2CH_2OH radicals absorb 266 nm light and dissociate to form OH.[3] In contrast, the survival fraction is smaller in our experiments, corresponding to only 85−89% of the radicals. The somewhat higher laser intensity at 266 nm in the present study could account for the higher fraction of dissociation. If the photodissociation of CH_2CH_2OH at 266 nm is independent of the internal energy, it is likely that some radicals in the I* channel will be photodissociated as well. Because the I* distribution in Figure 5 is scaled to the peak of the CH_2CH_2OH distribution, this result would imply that the 11−15% loss of radicals is a lower bound in our experiment. Nevertheless, the observation that the reconstruction in Figure 5 agrees with the high energy side of the CH_2CH_2OH radical distribution correlated with I $^2P_{3/2}$ atoms suggests that the 11−15% value for the fraction of dissociation may be very near the actual value. Independent of this conclusion, Figure 5 still indicates that a higher fraction of the radicals in the I channel dissociate than in the I* channel.

Anastasi et al.[16] have reported a uv absorption spectrum between 210 and 267 nm of the CH_2CH_2OH radical produced by radiolysis of an $Ar/SF_6/H_2O/C_2H_4$ sample. While the interpretation of such experiments can be difficult, the reported absorption cross section is greatest at the shortest wavelength measured, with a value of 2×10^{-18} cm^2/molecule at 210 nm. The absorption falls off nearly monotonically with increasing wavelength, plateauing at a minimum value of $\sim 2.5 \times 10^{-19}$ cm^2/molecule at approximately 260 nm. That spectrum was recorded at atmospheric pressure, however, so that the internal energy of the radical is likely significantly smaller than in the present experiments. Increased internal energy may shift the absorption to longer wavelengths, thus increasing the likelihood of absorption at 266 nm in the present experiments, particularly for radicals in the I channel. Because, on average, the radicals in the I channel have higher internal energy than those in the I* channel, this shift could account for the increased dissociation probability in the I channel. The enhancement of absorption in vibrationally excited radicals has recently been observed for CH_2Cl by Levchenko et al.[51]

Dissociative photoionization represents a second potential dissociation mechanism for CH_2CH_2OH in the present study. The ionization potential of the radical is thought to be $\leq 8.35 \pm 0.06$ eV (the experimental determination[49] was actually for CD_2CH_2OH), whereas the vuv photon energy corresponds to 10.486 eV, so that significant internal energy could be added to at least some fraction of the $CH_2CH_2OH^+$ ions. In the absence of a photoelectron spectrum for the radical (as well as the dependence of the photoelectron spectrum on the internal energy of the radical), the internal energy distribution is difficult to predict. In principle, however, there is also sufficient excess energy in the ionization photon to produce dissociative photoionization of the radicals formed in the I* channel as well. Unfortunately, the present experiment and analysis does not reveal the extent of fragmentation in the I* channel. Dissociative ionization should result in fragment ions at lower masses. However, the signal in the mass spectrum in the radical channel is quite weak already, and there is significant background from dissociative ionization of the parent 2-iodoethanol, so that no clear evidence for secondary ions was observed. Future work with lower energy vuv photons would help to resolve this issue. However, there is a large geometry change between the neutral CH_2CH_2OH radical and the corresponding ion (the neutral is thought to have a classical structure, while the ion is thought to have a cyclic structure), and the ionization cross section close to threshold is expected to be small. Thus, threshold photoionization may not be very effective for this radical, and the substantial internal energy of the radicals could have a significant impact on the threshold behavior, which may make it difficult to characterize.

C. Impulsive Rigid Radical Approximation. To assess the potential rotational excitation of the radical, the impulsive rigid radical model[24] was used to calculate the expected energy partitioning following the photodissociation of 2-iodoethanol in the Gg′ geometry calculated by Thomassen, Samdal, and Hedbert.[52] The Gg′ geometry corresponds to the structure in which the I atom is gauche (G) to the O atom and the hydroxy H is directed toward the I and gauche with the C bonded to I (g′) to form an internal H-bond. In the impulsive rigid radical model, the radical is rigid and there can be no vibrational excitation of the fragment. The rotational energy is then related to E_{avl} and E_{trans} by[24,53]

$$E_{avl} = E_{trans} + E_{rot} = E_{trans} + \frac{\mu_{R-I} b^2}{I_R} E_{trans} \quad (4)$$

where μ_{R-I} is the reduced mass of the R−I pair, b is the impact parameter of the I atom with respect to the center of mass of the radical, and I_R is the moment of inertia of the radical in the geometry of the parent molecule. With a known value of E_{avl}, the value of E_{trans} obtained from eq 4 is denoted E_{RR}, the total translational energy predicted by the rigid radical model. The Gg′ geometry of 2-iodoethanol[52] yields values of $b = 1.284$ Å for the impact parameter, $I_R = 52.08$ amu·Å^2 for the moment of inertia through the center of mass and perpendicular to the plane formed by the center of mass and the C−I bond, and 33.253 amu for the reduced mass. The use of eq 4 then gives $E_{RR}/E_{avl} = 0.49$, and the corresponding values of E_{RR} are noted in Figures 2 and 3. The predicted E_{RR} values are in reasonable agreement with the experimental values.

For dissociation to radicals correlated with ground state I, the experimental value of the energy partitioned into internal degrees of freedom is actually higher than that predicted by the rigid radical model. If the rigid radical model correctly predicts partitioning into rotational energy, then the difference between the amounts predicted by the model to be partitioned into translational energy and the experimentally measured values provides an estimate of the vibrational energies. For photodissociation at 258.687, 266.490, and 275.750 nm, this excess energy assigned to vibrational excitation is approximately 1300, 1000, and 1200 cm^{-1}. Photodissociation at 298.230 nm provides only about 400 cm^{-1} of vibrational excitation.

Although the rigid radical model does a remarkably good job of predicting the partitioning between internal and translational energy, the flexibility of the radical would suggest a significant amount of vibrational excitation upon photodissociation of the parent. For the same reason that rotational excitation is not effective at overcoming the dissociation barrier, one would also expect that rotational excitation would not enhance the photodissociation or dissociative photoionization of the radical. The observation that the radicals correlated with the I fragment are more susceptible to one of these processes than the radicals correlated with the I* fragment suggests that at least some fraction of the internal energy of the radicals corresponds to vibrational excitation.

V. Conclusions

Photodissociation of 2-iodoethanol to form 2-hydroxyethyl radical was initiated at several wavelengths resonant with the A band of alkyl halides and products observed via ion velocity-map imaging. Excitation to the $^3Q_{0+}$ state excited with a transition dipole parallel to the C−I bond dominates the spectrum in the wavelength region investigated. An I* branching fraction of $\Phi^* = 0.75 \pm 0.06$ at 266 nm was measured. Approximately half of the available energy was partitioned into internal degrees of freedom for radicals correlated with both I and I* atoms. The rigid radical model of the dissociation provides good agreement with the observed partitioning between translational and internal energies and suggests the radicals are produced in highly excited rotational states. However, a large fraction (45−60%) of the I-correlated radicals from 266 nm photodissociation of 2-iodoethanol underwent secondary dissociation as a result of photodissociation or dissociative photoionization. The present results suggest two types of experiments for future study. First, experiments on the photodissociation and photoionization of cold C_2H_4OH radicals produced by photodissociation or pyrolysis in the supersonic expansion would allow a better characterization of the absorption by the radical itself. Such experiments have recently allowed a detailed characterization of the spectroscopy and dynamics of the 1-hydroxyethyl radical.[54] Second, experiments with lower energy vuv photons would allow a better understanding of dissociative ionization processes. Efforts to combine these two improvements are currently underway.

Acknowledgment. We would like to thank Professors L. J. Butler and H. Reisler for helpful discussions regarding this study. We would also like to thank Dr. S. J. Klippenstein for sharing his results on C_2H_4OH. This work was supported by the U.S. Department of Energy, Office of Science, Office of Basic Energy Sciences, Division of Chemical Sciences, Geosciences, and Biosciences under Contract No. DE-AC02-06CH11357. M.R. was supported by funding through the University of Chicago/Argonne Strategic Collaborative Initiative.

References and Notes

(1) Bott, J. F.; Cohen, N. *Int. J. Chem. Kinet.* **1991**, *23*, 1075.
(2) Ruscic, B.; Berkowitz, J. *J. Chem. Phys.* **1994**, *101*, 10936.
(3) Sapers, S. P.; Hess, W. P. *J. Chem. Phys.* **1992**, *97*, 3126.
(4) Tully, F. P. *Chem. Phys. Lett.* **1983**, *96*, 148.
(5) Tully, F. P. *Chem. Phys. Lett.* **1988**, *143*, 510.
(6) Raman, A. S.; Bell, M. J.; Lau, K. C.; Butler, L. J. *J. Chem. Phys.* **2007**, *127*, 154316.
(7) Senosiain, J. P.; Klippenstein, S. J.; Miller, J. A. *J. Phys. Chem. A* **2006**, *110*, 6960.
(8) Hippler, H.; Viskolcz, B. *Phys. Chem. Chem. Phys.* **2000**, *2*, 3591.
(9) Liu, G. X.; Ding, Y. H.; Li, Z. S.; Fu, Q.; Huang, X. R.; Sun, C. C.; Tang, A. C. *Phys. Chem. Chem. Phys.* **2002**, *4*, 1021.
(10) Zhu, R. S.; Park, J.; Lin, M. C. *Chem. Phys. Lett.* **2005**, *408*, 25.
(11) Yamada, T.; Bozzelli, J. W.; Lay, T. *J. Phys. Chem. A* **1999**, *103*, 7646.
(12) Bernardes, C. E. S.; da Piedade, M. E. M.; Amaral, L. M. P. F.; Ferreira, A. I. M. C. L.; da Silva, M. A. V. R.; Diogo, H. P.; Cabral, B. J. C. *J. Phys. Chem. A* **2007**, *111*, 1713.
(13) Matsunaga, A.; Ziemann, P. J. *J. Phys. Chem. A* **2009**, *113*, 599.
(14) Chandler, D. W.; John, W.; Thoman, J.; Hess, W. P. *Inst. Phys. Conf. Ser. No. 114: Section 8* **1990**, 355.
(15) Hintsa, E. J.; Zhao, X. S.; Lee, Y. T. *J. Chem. Phys.* **1990**, *92*, 2280.
(16) Anastasi, C.; Simpson, V.; Munk, J.; Pagsberg, P. *J. Phys. Chem.* **1990**, *94*, 6327.
(17) Aguirre, F.; Pratt, S. T. *J. Chem. Phys.* **2005**, *122*, 234303.
(18) Aguirre, F.; Pratt, S. T. *J. Chem. Phys.* **2003**, *118*, 1175.
(19) Eppink, A. T. J. B.; Parker, D. H. *Rev. Sci. Instrum.* **1997**, *68*, 3477.
(20) Dribinski, V.; Ossadtchi, A.; Mandelshtam, V. A.; Reisler, H. *Rev. Sci. Instrum.* **2002**, *73*, 2634.
(21) Garcia, G. A.; Nahon, L.; Powis, I. *Rev. Sci. Instrum.* **2004**, *75*, 4989.
(22) Mulliken, R. S. *J. Chem. Phys.* **1940**, *8*, 382.
(23) Mulliken, R. S. *Phys. Rev.* **1942**, *61*, 277.
(24) Riley, S. J.; Wilson, K. R. *Discuss. Faraday Soc.* **1972**, *53*, 132.
(25) Schinke, R. *Photodissociation Dynamics*; Cambridge University: New York, 1993.
(26) Gedanken, A.; Rowe, M. D. *Chem. Phys. Lett.* **1975**, *34*, 39.
(27) Donohue, T.; Wiesenfeld, J. R. *J. Chem. Phys.* **1975**, *63*, 3130.
(28) Sparks, R. K.; Shobatake, K.; Carlson, L. R.; Lee, Y. T. *J. Chem. Phys.* **1981**, *75*, 3838.
(29) Guo, H.; Schatz, G. C. *J. Chem. Phys.* **1990**, *93*, 393.
(30) Guo, H.; Lao, K. Q.; Schatz, G. C.; Hammerich, A. D. *J. Chem. Phys.* **1991**, *94*, 6562.
(31) Rist, C.; Alexander, M. H. *J. Chem. Phys.* **1993**, *98*, 6196.
(32) Amatatsu, Y.; Morokuma, K.; Yabushita, S. *J. Chem. Phys.* **1991**, *94*, 4858.
(33) Amatatsu, Y.; Yabushita, S.; Morokuma, K. *J. Chem. Phys.* **1996**, *104*, 9783.
(34) Eppink, A. T. J. B.; Parker, D. H. *J. Chem. Phys.* **1998**, *109*, 4758.
(35) Eppink, A. T. J. B.; Parker, D. H. *J. Chem. Phys.* **1999**, *110*, 832.
(36) Fan, H. Y.; Pratt, S. T. *J. Chem. Phys.* **2005**, *123*, 204301.
(37) Alekseyev, A. B.; Liebermann, H. P.; Buenker, R. J. *J. Chem. Phys.* **2007**, *126*, 234103.
(38) Alekseyev, A. B.; Liebermann, H. P.; Buenker, R. J. *J. Chem. Phys.* **2007**, *126*, 234102.

(39) Han, J. C.; Suto, M.; Lee, L. C. *J. Quant. Spectrosc. Radiat. Transfer* **1989**, *42*, 557.

(40) Herzberg, G. *Molecular Spectra and Molecular Structure III. Electronic Spectra and Electronic Structure of Polyatomic Molecules*; Krieger Publishing Company: Malabar, FL, 1966.

(41) Minnhagen, L. *Ark. Fys.* **1962**, *21*, 415.

(42) Li, G. S.; Shin, Y. K.; Hwang, H. J. *J. Phys. Chem. A* **2005**, *109*, 9226.

(43) Zhu, Q. H.; Cao, J. R.; Wen, Y.; Zhang, J. M.; Zhong, X. A.; Huang, Y. H.; Fang, W. Q.; Wu, X. J. *Chem. Phys. Lett.* **1988**, *144*, 486.

(44) Zhang, X.-P.; Lee, W.-B.; Lin, K.-C. *J. Phys. Chem. A* **2009**, *113*, 35.

(45) Tang, Y.; Lee, W. B.; Hu, Z. F.; Zhang, B.; Lin, K. C. *J. Chem. Phys.* **2007**, *126*, 064302.

(46) Xu, X. L.; Yu, Z. J.; Bi, W. B.; Xiao, D. Q.; Yu, D.; Du, Y. K.; Zhu, Q. H. *J. Phys. Chem. A* **2008**, *112*, 1857.

(47) Suits, A. G. *Acc. Chem. Res.* **2008**, *41*, 873.

(48) Klippenstein, S. J. Private communication, 2009.

(49) Ruscic, B.; Berkowitz, J. *J. Chem. Phys.* **1994**, 10936.

(50) National Institute of Science and Technology Chemistry WebBook at http://webbook.nist.gov/.

(51) Levchenko, S. V; Demyanenko, A. V; Dribinski, V. L; Potter, A. B; Reisler, H.; Krylov, A. I. *J. Chem. Phys.* **2003**, *118*, 9233.

(52) Thomassen, H.; Samdal, S.; Hedberg, K. *J. Phys. Chem.* **1993**, *97*, 4004.

(53) Fan, H.; Pratt, S. T. J. *Chem. Phys.* **2006**, *124*, 144313.

(54) Karpichev, B.; Edwards, L. W.; Wei, J.; Reisler, H. *J. Phys. Chem. A* **2008**, *112*, 412.

JP903301G